JOURNAL OF GEOPHYSICAL RESEARCH, VOL. 99, NO. C6, PAGES 12,357–12,373, JUNE 15, 1994

Spin-up and breakdown of source-driven deep North Atlantic flow over realistic bottom topography

Michael Karcher and Angelika Lippert

Institut für Meereskunde, Universität Hamburg, Germany

Abstract. In this study we examine the time dependent behaviour of the deep North Atlantic dynamics. We use a $1\frac{1}{2}$-layer, nonlinear, shallow water model with realistic topography and high-spatial resolution. It is driven by an inflow of deep water from a northern source and by parameterized density exchange processes at the interface. The evolving circulation pattern is complex. The Mid–Atlantic Ridge with the Charlie Gibbs Fracture Zone has a fundamental influence on the large-scale flow field. A reduction of the inflow causes a temporary reversal of the interior currents. The perturbation travels along the geostrophic contours. The response times of the currents for the spin-up and breakdown experiments are of the order of years. They differ for different areas of the North Atlantic Ocean. The area which is affected last by the perturbation is the northwesternmost interior corner, which is close to the position of the source.

Introduction

In recent years a number of process studies have used simplified layer models to investigate different aspects of the deep oceanic circulation. The basic reference for all deep circulation models is the work of *Stommel and Arons* [1960]. They calculate the steady state motion of water in the abyss by means of an analytical model ocean of constant depth that is driven by a uniform upwelling at its upper boundary. This forcing is motivated by a global balance between sinking water in polar regions and upwelling elsewhere. The resulting flow in the interior ocean is poleward toward the source. Stommel and Arons postulated a deep current along the western boundary which feeds the poleward interior flow. The existence of this Deep Western Boundary Current (DWBC) has been confirmed by numerous measurements [e.g., *Swallow and Worthington*, 1961; *Hogg*, 1983].

Most investigators following the basic ideas of *Stommel and Arons* [1960] assume a balance between upwelling and vertical diffusion of density at the top of the deep layers. *Tziperman* [1986] discusses the impact of this small-scale process for the steady state general circulation. This process not only provides a forcing or stirring of the circulation but also plays a crucial part in determining the basic density stratification of the ocean. Several authors discuss the different processes affecting the steady state and the spin-up of the deep flow. *Welander* [1969] tried to obtain a qualitative picture of the topographic impact on the steady deep flow of the Stommel-Arons model. Regions of closed geostrophic contours, a meridional ridge or realistic topography gave rise to interior jets and intense recirculations. *Kawase* [1987] shows how the steady state flow depends on the magnitude of the density flux across the interface of a $1\frac{1}{2}$-layer ocean. The combined effect on the steady state flow of wind, buoyancy, and topography is adressed by *Hautala and Riser* [1989].

Kawase [1987] also studied the evolution of the deep-flow pattern in a flat bottom ocean of rectangular shape which is driven by an inflow of mass from the northwest. Subsequently, *Straub and Rhines* [1990], *Kawase and Straub* [1991], *Condie and Kawase* [1992], and *Kawase* [1993] studied deviations from the flat bottom spin-up case as a consequence of modified characteristics with simplified topographies.

This study goes a step further by focusing on the impact of a more realistic topography on the spin-up and the breakdown of a source-driven deep North Atlantic current field. We use a $1\frac{1}{2}$-layer, nonlinear, shallow water model driven by an inflow of deep water from northern sources and by parameterized density exchange processes at the interface.

The spin-up of the deep flow is performed by coastal and equatorial Kelvin and Rossby waves. The stationary flow pattern exhibits significant differences from the classical Stommel-Arons picture of the abyssal circulation in particular, an intense northward current along the Mid-Atlantic Ridge develops which is connected to an eastern boundary current by zonal interior flows. Experiments with an idealized meridional ridge reveal that the existence of a gap at northern latitudes is responsible for the northward ridge current. A strong reduction of one of the sources effects the breakdown of the steady state circulation. The adaptation to another

Paper number 94JC00529.
0148-0227/94/94JC-00529$05.00

equilibrium state is initiatized. During this adaptation the response timescales differ geographically. They are determined by the typical timescales of the baroclinic coastal and equatorial Kelvin waves and Rossby waves participating in the adjustment process and are of the order of months to years. These timescales are short compared to those associated with measured changes of the mass field in parts of the deep North Atlantic [e.g., *Roemmich and Wunsch*, 1984; *Levitus*, 1989] which are of the order of decades, and in particular, they are short compared with changes of the global mass field which are in the order of centuries.

The Model

The model is based on the vertically integrated shallow water equations in Boussinesq approximation. It consists of one moving layer of density ρ_2 that represents the abyss and a stagnant upper layer of density ρ_1. The moving layer is driven by an inflow of dense water into the lower layer at the northern boundary, which represents the northern deep water sources of the Atlantic Ocean. Between the two layers a cross-interfacial flux of density balances the diapycnal diffusion of density. The nonlinear momentum equations include a lateral eddy viscosity and a linear bottom stress.

Equations of Motion

The equations for the vertically averaged horizontal velocities hold

$$\frac{\partial u}{\partial t} - (f+\zeta)v = -\frac{1}{R_0\cos\theta}\frac{\partial}{\partial\phi}\left(g'\eta + \frac{1}{2}(u^2+v^2)\right) - Fu + A_h\left(\nabla^2 u + \frac{(1-\tan^2\theta)}{R_0^2}u - \frac{2\sin\theta}{R_0^2\cos^2\theta}\frac{\partial v}{\partial\phi}\right) \quad (1)$$

$$\frac{\partial v}{\partial t} + (f+\zeta)u = -\frac{1}{R_0}\frac{\partial}{\partial\theta}\left(g'\eta + \frac{1}{2}(u^2+v^2)\right) - Fv + A_h\left(\nabla^2 v + \frac{(1-\tan^2\theta)}{R_0^2}v + \frac{2\sin\theta}{R_0^2\cos^2\theta}\frac{\partial u}{\partial\phi}\right) \quad (2)$$

Where u, v are the components of velocity in eastern ($\hat{\phi}$) and northern ($\hat{\theta}$) directions respectively, η is the displacement of the interface relative to its initial value, g' is the reduced gravity and $f = 2\Omega\sin\theta$ is the Coriolis parameter. F and A_h denote the coefficients for linear bottom friction and horizontal viscosity. The gradient operator ∇ is taken in spherical coordinates. Here ζ is the relative vorticity:

$$\zeta = 1/(R_0\cos\theta)\left(\frac{\partial v}{\partial\phi} - \frac{\partial(u\cos\theta)}{\partial\theta}\right). \quad (3)$$

Equation of Continuity

Vertical integration of the continuity equation for a layer model leads to [*Simons*, 1980]:

$$\frac{\partial D}{\partial t} + \nabla\cdot(D\vec{v}) + e_{k-1} - e_k = S(\phi,\theta) \quad (4)$$

where k is an interface index counting downward, $D = H + \eta$ is the total layer depth and $S(\phi,\theta)$ is a source term. The volume flux through the interface k is given by

$$e_k \equiv w_k - \vec{v}\nabla z_k - \frac{\partial z_k}{\partial t}, \quad (5)$$

where w_k is the upward ($\hat{z}$) component of velocity at the kth interface. If $e_k = 0$, the interface is impermeable. At the bottom $k = H$ where e_H and $\frac{\partial z_H}{\partial t}$ are both identically zero, the kinematic boundary condition holds

$$w_H = \vec{v}\nabla z_H. \quad (6)$$

Density Conservation and Flux Through the Interface

In the following derivation of e we make use of the conservation of density provided by a balance between diapycnal advection and diffusion of density. Note that in this model there is no diffusion or advection along the interface.

The balance is expressed by the equation for the conservation of density at the interface, which reads

$$e\frac{\partial\rho}{\partial n} = k_d\frac{\partial^2\rho}{\partial n^2}, \quad (7)$$

where n is the distance normal to the interface, k_d is the coefficent of the diapycnal diffusion, and the subscripts have been dropped.

Tziperman [1986] gave the following expression for $\frac{\partial^2\rho}{\partial n^2}/\frac{\partial\rho}{\partial n}$ in a layer model. The lth layer represents the density range between ρ_a and ρ_b, $\Delta_l\rho = \rho_a - \rho_b$ is the density range. The density of the layer is $\rho_l = (\rho_a + \rho_b)/2$, its thickness is D_l.

$$\frac{\partial^2\rho}{\partial n^2}/\frac{\partial\rho}{\partial n} = \frac{\Delta_{l+1}\rho/D_{l+1} - \Delta_l\rho/D_l}{\rho_{l+1} - \rho_l} \quad (8)$$

It is possible to linearize this expression, and for a two-layer case, $(l = 1,2), D_1 = H_1 - \eta, D_2 = H_2 + \eta$, the result is

$$\frac{\partial^2\rho}{\partial n^2}/\frac{\partial\rho}{\partial n} \approx \frac{\Delta_1\rho}{(\rho_2-\rho_1)H_1} + \frac{\Delta_1\rho}{(\rho_2-\rho_1)H_1^2}\eta \quad (9)$$

where H_1 is the undisturbed upper-layer thickness. The first term on the right is constant, whereas the second term, linear in η, represents a Rayleigh damping (respectively Newtonian cooling). Substitution of (9) into (7) gives

$$e = e_0 + \lambda\eta \quad (10)$$

with

$$\lambda = k_d\frac{\Delta_1\rho}{(\rho_2-\rho_1)H_1^2} \quad (11)$$

$$e_0 = k_d\frac{\Delta_1\rho}{(\rho_2-\rho_1)H_1}. \quad (12)$$

Equation (10) gives an interface flux that is composed of a constant term and a variable term that is entirely

determined by the flow. Thus, substituting (10), equation (4) obtains its final form

$$\frac{\partial \eta}{\partial t} + \nabla \cdot (D\vec{v}) + e_0 + \lambda\eta = S(\phi, \theta) \qquad (13)$$

We are well aware of the fact that the parameterization of small-scale turbulence analogous to molecular diffusion is crude [*Pedlosky*, 1987]. Besides, the vertical diffusion coefficient k_d is usually assumed constant in time and uniform in space in numerical models of oceanic flow. This assumption seems not to be supported by observational evidence [*Gargett*, 1984; *Gregg*, 1987]. Varying k_d horizontally leads to nonuniform upwelling and profoundly affects the Stommel-Arons pattern of deep interior flow [*Karcher et al.*, 1990]. Since the focus of this paper is specifically on the effects of bottom topography, the following experiments are based on the assumption of a spatially constant k_d. In addition, this simplifies comparison with investigations by other authors.

Topography

We use the realistic topography of the North Atlantic below 1000 m. Closed boundary conditions are applied along the 1000 m isobath. An open southern boundary is placed at 25°S. Altough the focus of this study lies on the North Atlantic flow, the low-latitude South Atlantic had to be included into the model area. *Kawase* [1987] highlights the importance of the equator for the onset of the midlatitude circulation. Our investigations showed that the distance of the open boundary to the equator should at least be 25°. Otherwise the solutions will be distorted even north of the equator. The bottom relief is taken from the SYNBAPS (Synthetic Bathymetric Profiling System) data averaged to 0.5° and interpolated on a 0.25° grid (Figures 1 and 2). Adjacent basins like the Gulf of Mexico have not been included in the model domain.

Numerical Integration

The time integration starts from an ocean at rest. A leapfrog scheme with a time step of 30 minutes is employed. Enstrophy-conserving finite difference analogs to the model equations are formulated on an Arakawa C grid [*Sadourny*, 1975]. The same procedure was applied in the model of *Kawase and Straub* [1991]. Boundary conditions specify zero normal flow and free slip tangential flow at the closed boundaries. The gradient of the meridional velocity normal to the boundary is assumed to be zero at the open boundary in the south. An increase of the friction coefficient in the vicinity of the southern boundary prohibits reflection of information back into the model domain.

Parameter Choices

For the adjustment we need to resolve the first-mode Rossby radius of deformation R_{def}. Otherwise the essential Kelvin waves are misrepresented. We chose a spatial resolution of $\Delta_{\text{grid}} = 0.25°$. This gives a minimum zonal grid size of 11.7 km at 65°N and a meridional grid step of 27.8 km. The initial depth of the interface is 1000 m. In areas where the depth is shallower than 2000 m the bottom slope has been reduced to one fifth of its original value. Thus a minimum of the resolution of the Rossby deformation radius $Res = R_{\text{def}}/\Delta_{\text{grid}} = 1$ is ensured. The resolution is $Res < 2$, however, only in very narrow zones along the boundaries. The decay time for the bottom friction is $F^{-1} = 15$ days, the horizontal viscosity coefficient is $A_h = 200\ m^2/s$, and the reduced gravity is $g' = 5 \times 10^{-3}\text{m/s}^2$. The density stratification is chosen as $\Delta_1\rho/\Delta_2\rho = 10$ and the background value of the cross-interfacial velocity as $e_0 = 1.3 \times 10^{-7}\text{m/s}$. We use a vertical diffusion coefficient of $k_d = 2 \times 10^{-3}\text{m}^2/\text{s}$, which gives a damping timescale of ≈ 3000 days for the long baroclinic Rossby waves (see the appendix).

Spin-up

The spin-up of the North Atlantic from rest is forced by two deep-water sources. For the model, 8.6 Sv (1 Sv = $1 \times 10^6\text{m}^3/\text{s}$) are injected at the model's "Denmark Strait" and 4.1 Sv represent the overflow between Iceland and Scotland. The inflow increases gradually from zero to its terminal strength of 12.7 Sv within 50 days. Both inflows have much greater volume fluxes than observed. However, observations also suggest that the volume flux of the plume grows downstream owing to entrainment of ambient water [*Dickson et al.*, 1990, *Saunders*, 1990]. Since our model does not contain entrainment physics, the plume is made large to start with.

Figures 3a–3d show the interface displacement after 50, 100, 200, and 400 days of inflow, and each picture represents a new stage of development. First a boundary current evolves in the wake of a coastal Kelvin wave that moves westward as the Deep Northern Boundary Current (DNBC) and equatorward as the DWBC (Figure 3a). Then the signal crosses the ocean along the equator in the form of an equatorial Kelvin wave (Figure 3b). As it hits the eastern boundary it splits into two coastal Kelvin waves traveling poleward and forming eastern boundary currents in both hemisperes. These boundary currents generate long Rossby waves which travel westward and build up the interior circulation (Figures 3c and 3d). The group velocity of the Rossby wave $v_{gr} = \beta R_{\text{def}}^2$ decreases with the latitude, so the circulation seems to develop from the equator toward the poles. The Rossby waves dissipate, and after about 10 years the flow field becomes stationary. During the final adjustment the interface sinks uniformly until the flux through the interface balances the deficit of inflow and outflow.

On day 200 (Figure 3c) the excitation of the long Rossby waves is noticable. South of 20°N the Rossby wave has reached the American continent, whereas along the European coastline the signal is still attached to the eastern boundary. At this stage of evolution a continuous deep western boundary current south of the equator has not yet developed.

The Rossby wave that has penetrated the interior ocean on day 400 (Figure 3d) is obviously associated

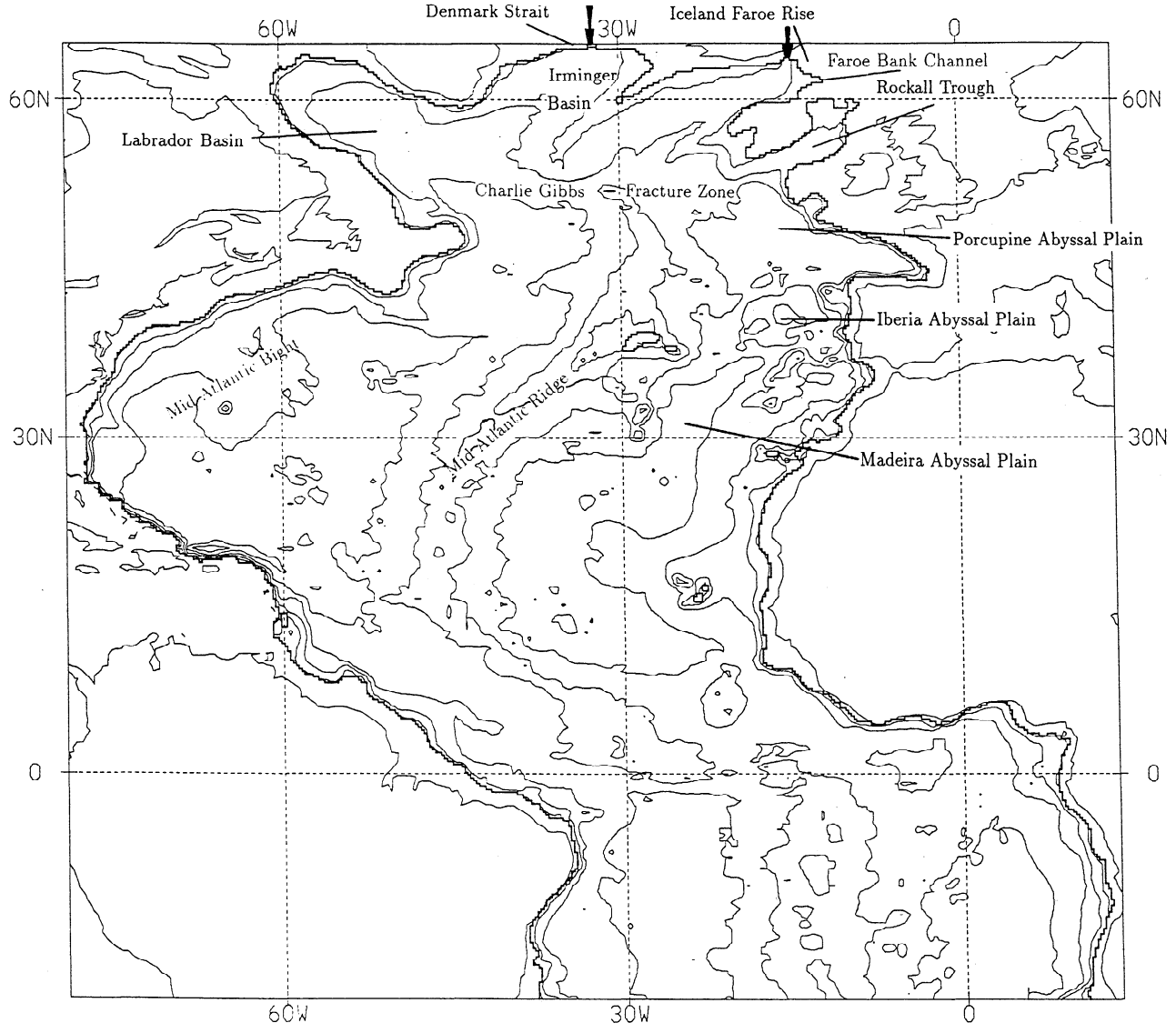

Figure 1. Topography of the model area between 65°N and 20°S. The contour interval is 1000 m and the perimeter of the basin follows the 1000 m contour. The arrows indicate the inflow areas.

with a strong inclination of the interface and high poleward velocities. At low latitudes the Mid-Atlantic Ridge causes a sharp turn of the high-velocity belt in the North Atlantic. The width of the DWBC varies as it moves south. At low latitudes south of the equator the Rossby wave has arrived at the western boundary. A southern continuation of the DWBC is now established.

This sequence of the spin-up process is very similiar to the stages of development that *Kawase* [1987] found in a model of the abyssal ocean with flat bottom and rectangular shape driven by a source of mass at the western boundary. In contrast to his model, here the orientation of the high-velocity belt depends not only on the distance to the equator but also on the orientation of the eastern coastline and the specific control by the geostrophic contours (see Figure 2). The strong currents change direction while moving west with the Rossby wave. In some areas the flow is even opposite to the flat bottom flow. The DWBC is accompanied by several recirculation cells and bifurcations, most of which are still present when the steady state is reached.

Steady state

We define the steady state by an upper bound for the rate of interface displacement change of 1×10^{-4} m/d. The model reaches this after 9600 days of integration. The illustrations of the interface displacement (Figure 4a) and the velocity field (Figure 4b) reveal the complex structure of the steady state circulation. One of the most conspicious features of the large-scale circulation is a cyclonic recirculation gyre encompassing the whole

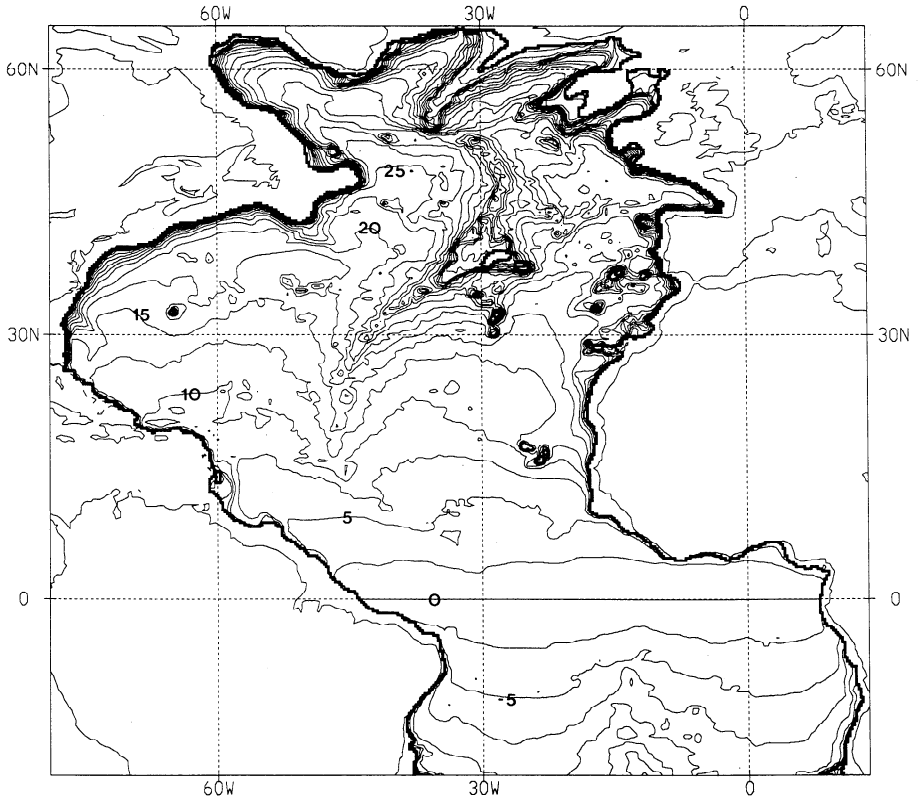

Figure 2. Contours of constant f/H (geostrophic contours, H, depth). The contour labels give the isoline values in units of $10^{-9}(\mathrm{sm})^{-1}$ at an interval of $2.5 \times 10^{-9}(\mathrm{sm})^{-1}$.

western basin of the North Atlantic. Medium-scale cyclonic gyres have developed in the Labrador basin interior, off Newfoundland, and in the Mid-Atlantic Bight. Most of the visible small-scale flow patterns are induced by local topographic features. The small recirculation cell in the Rockall Trough could be an artifact, introduced by the reduction of the bottom slope that changes the local curvature of the f/H contours.

Between 30°N and 10°N a fraction of the DWBC separates from the coast, turning southeastward toward the Mid-Atlantic Ridge. Part of it crosses the ridge and turns north in a sharp bow to follow its eastern flank poleward. This trapped ridge current intensifies on its way north, and at the Charlie Gibbs Fracture Zone (CGFZ) it moves back into the western basin to rejoin the DNBC in the Irminger Basin. Several branches of this ridge current leave the slope in midlatitude, and merge into a poleward eastern boundary current along the continental slope. Part of the DWBC moves along the equator in small-amplitude meanders. The widening of the DWBC near the southern boundary is a consequence of the enhanced friction close to this boundary.

A total volume of 16.3 Sv crosses a section perpendicular to the DWBC at 35°N, leaving 3.6 Sv for the recirculation cell, compared to the inflow of 12.7 Sv. A volume of 8.5 Sv crosses the equator. Thus in the northern hemispere 4.2 Sv leave the deep layer across the interface.

Role of the CGFZ for the Poleward Ridge Current

The most pronounced feature of the interior model circulation is the poleward ridge current on the eastern slope of the Mid-Atlantic Ridge. It extends all along the ridge. Its direction is opposite to that in several other studies that investigate the influence of a meridional ridge on the circulation pattern. *Condie and Kawase* [1992] compared the spin-up and the steady state in a $1\frac{1}{2}$-layer box-shaped numerical model with a laboratory experiment. Both have a meridional ridge in combination with a concave bottom topography in the vicinity of the boundaries. When driven by a source located in the northwest corner of the basin, both experiments show an equatorward flow along the eastern slope and a poleward flow along the western slope of the ridge. Across the ridge, water is leaking from the eastern into the western basin. It is important to note that their model does not include the equator and their southern boundary is closed.

If the boundaries are vertical walls instead, a jet develops in the interior western basin which links the western boundary current with a current along the closed southern boundary (M. Kawase, personal communication, 1991). This jet has been described by *Cessi and Pedlosky* [1986] as a discontinuity in the interface height, a result of two converging geostrophic contours

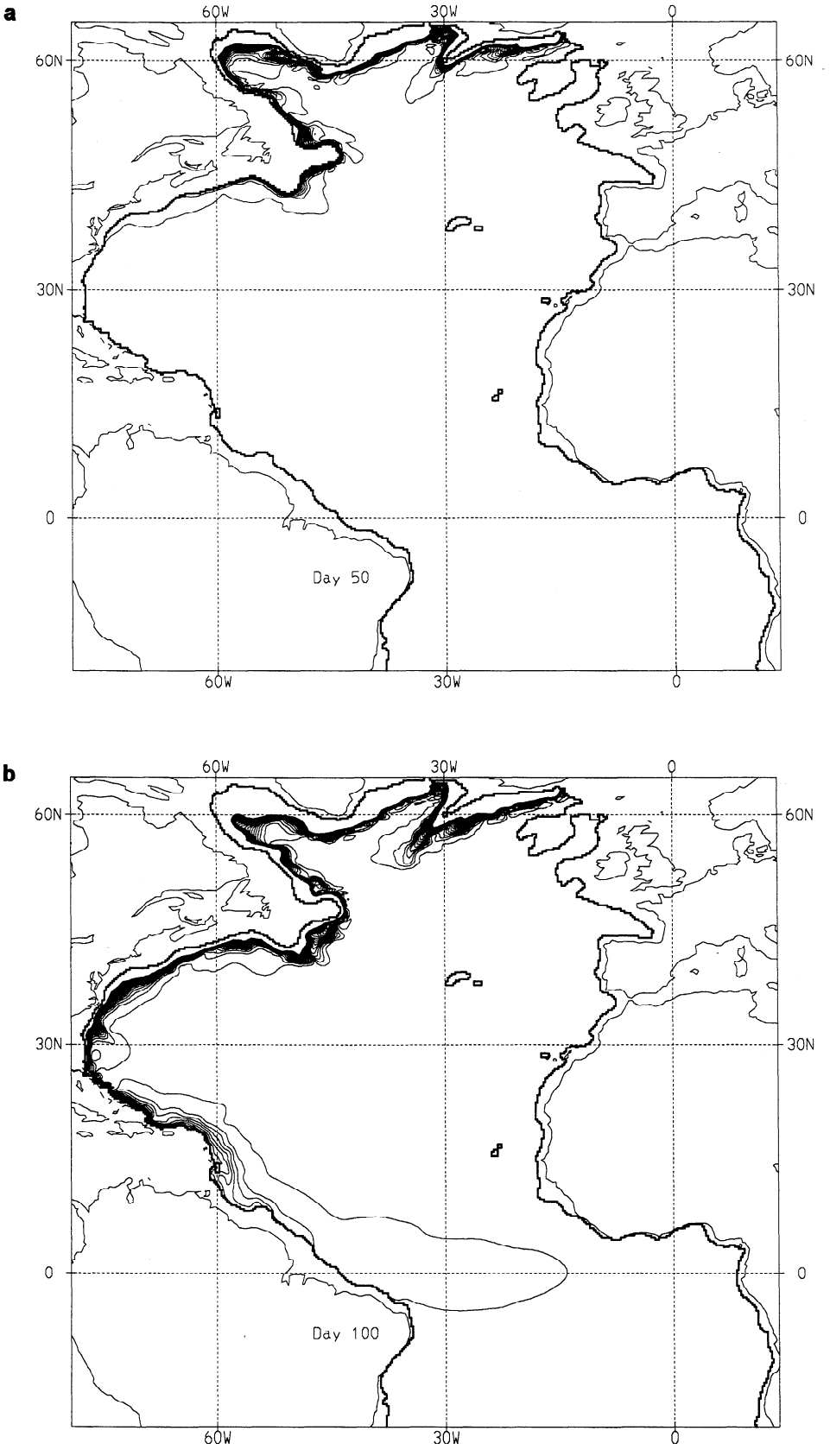

Figure 3. The spin-up. Lines of constant interface displacement relative to 1000 m depth. The contour interval is 0.5 m and lines in excess of 10 m have been omitted. (a) day 50, (b) day 100, (c) day 200, and (d) day 400.

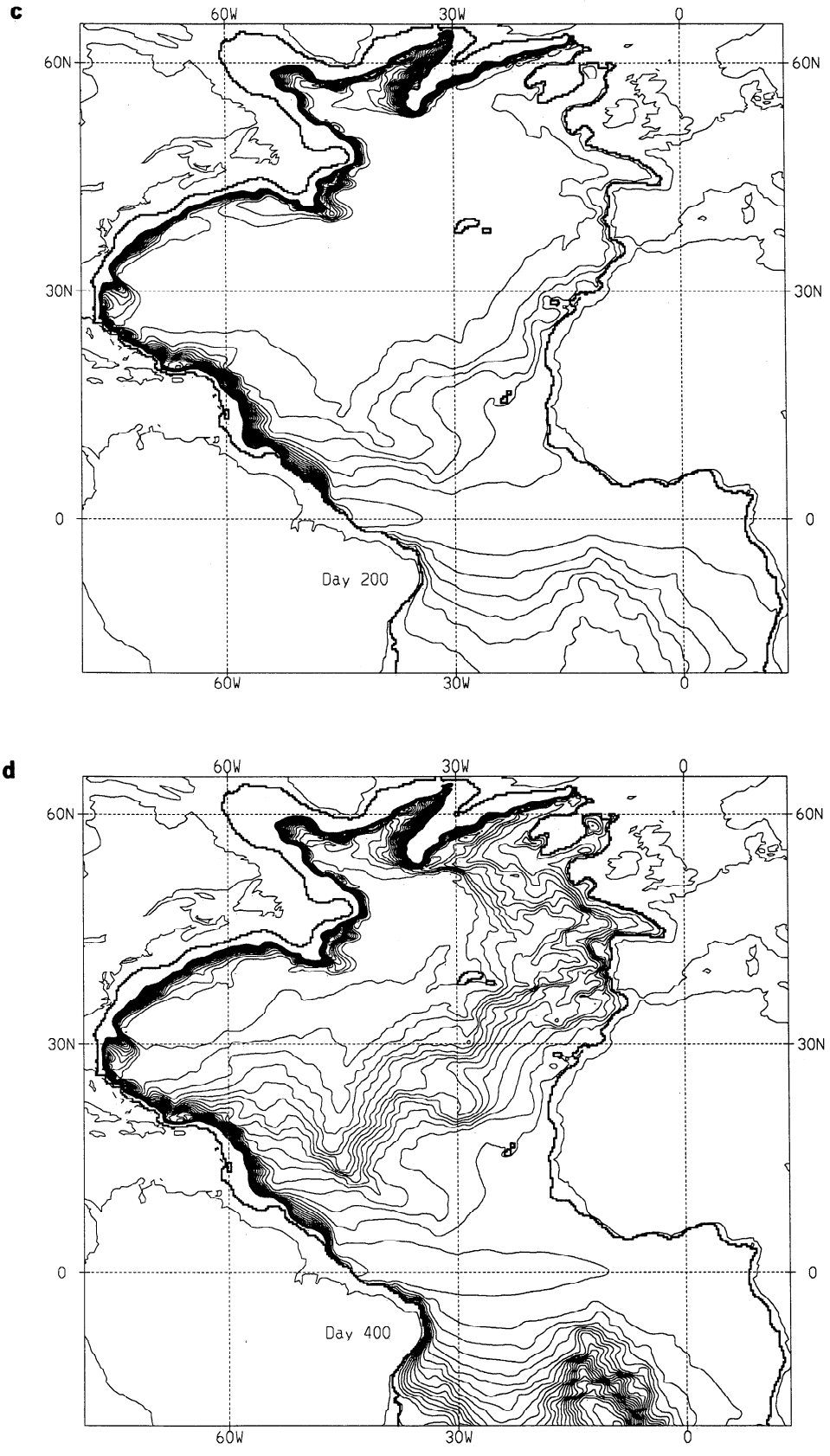

Figure 3. (continued)

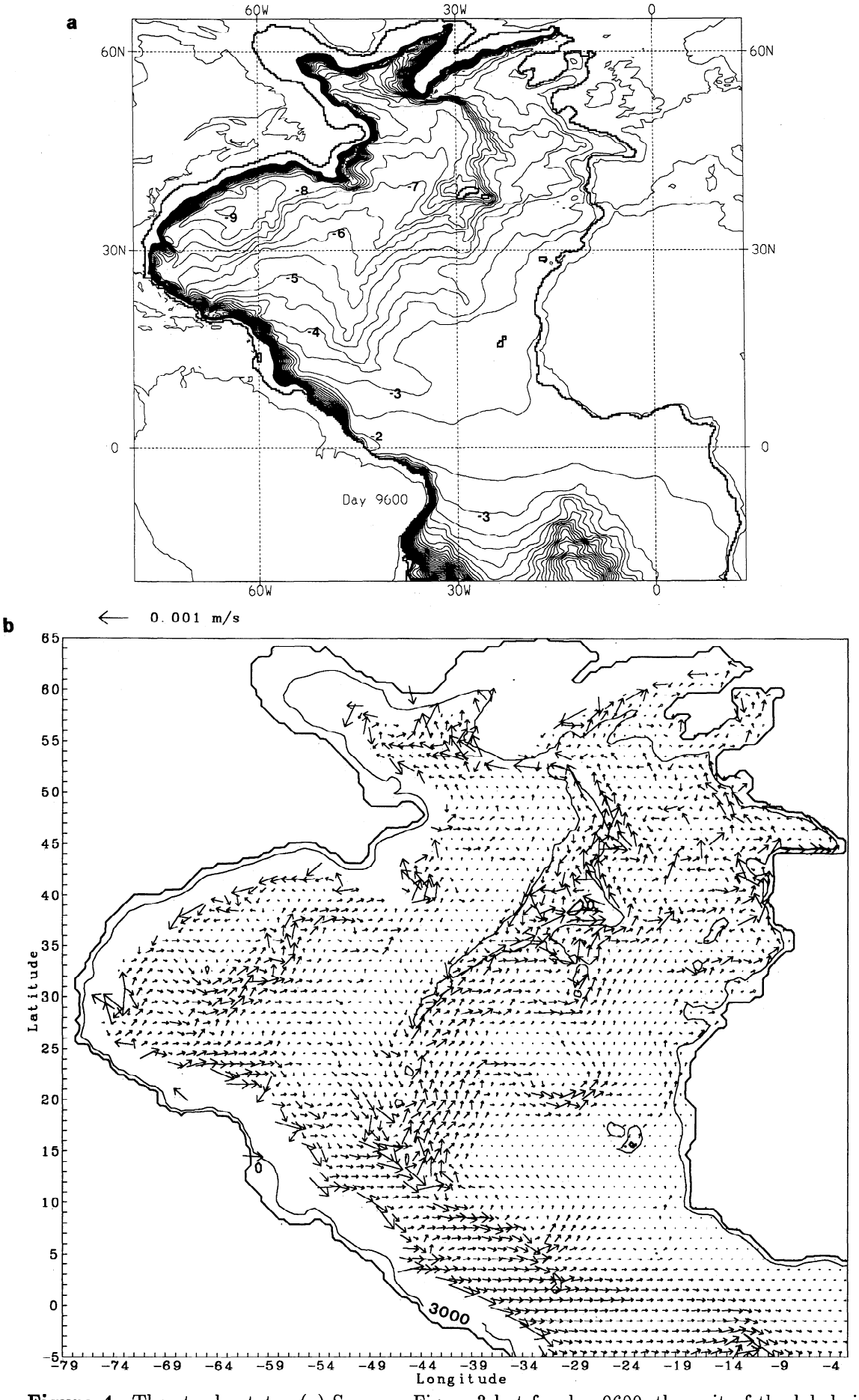

Figure 4. The steady state. (a) Same as Figure 3 but for day 9600, the unit of the labels is meters. (b) Current velocities on day 9600. The thin line is the 3000 m depth contour. Every fourth data point has been plotted and current velocities in excess of 1×10^{-3}m/s have been omitted.

with origins far apart. One of them starts at the intersection of the ridge with the southern boundary and the other at high latitude on the eastern boundary. However, when the model domain extends across the equator and the southern boundary is open, the interior jet disappears and the velocity on the slopes of the ridge is intensified, a fact that has already been described qualitatively by *Welander* [1969]. The equatorward flow leaks across the ridge, and the flow is poleward south of a latitude where all the water has moved into the western basin. These studies, however, do not consider the existence of a gap in the ridge at high latitudes such as the CGFZ in the Mid-Atlantic Ridge.

In fact, this gap induces the poleward ridge current which can be seen in Figures 4a and 4b. To illustrate this, we performed two experiments with a box-shaped ocean enclosed by vertical walls, an open southern boundary, and a meridional ridge of Gaussian shape. The ridge rises 1000 m above the flat bottom of 3000 m depth and has an e-folding scale of 5°. The model domain has a width of 40° and extends from 50°N to 30°S. The inflow has been set to 6 Sv, all other parameters kept the values of the realistic topography case. Figure 5a shows the interface height for the steady state (day 10800). The interface displacement pattern is similiar to that found by *Welander* [1969]. Figure 5b, on the other hand, shows the results of an experiment with a gap in the ridge representing the CGFZ. Obviously, the distortion of the geostrophic contours by the gap (Figure 6a and 6b) induces poleward flow all along the eastern slope of the ridge between the gap and the equator. The jet intensifies poleward and is supplied by water coming from the DWBC, just as in the realistic topography case. As a consequence of these simple experiments a number of questions on the deep-flow dynamics arise that have not been adressed before. They concern the role of the fracture zones and in particular the CGFZ. It is beyond the scope of this paper to answer these questions. They will be the subject of a separate investigation currently under preparation.

Comparison With Data

It cannot be expected that the present model, developed for process studies, be able to simulate details of the observed abyssal current field. Nevertheless, some features of the observed flow field in parts of the North Atlantic are clearly identifiable in the numerical results.

From hydrographic data, *McCartney et al.* [1991] and *McCartney* [1992] inferred the path of water entering the eastern basin through the Vema Fracture Zone in the Mid-Atlantic Ridge (at ≈11°N). This flow follows the ridge along its eastern flank as a western intensified

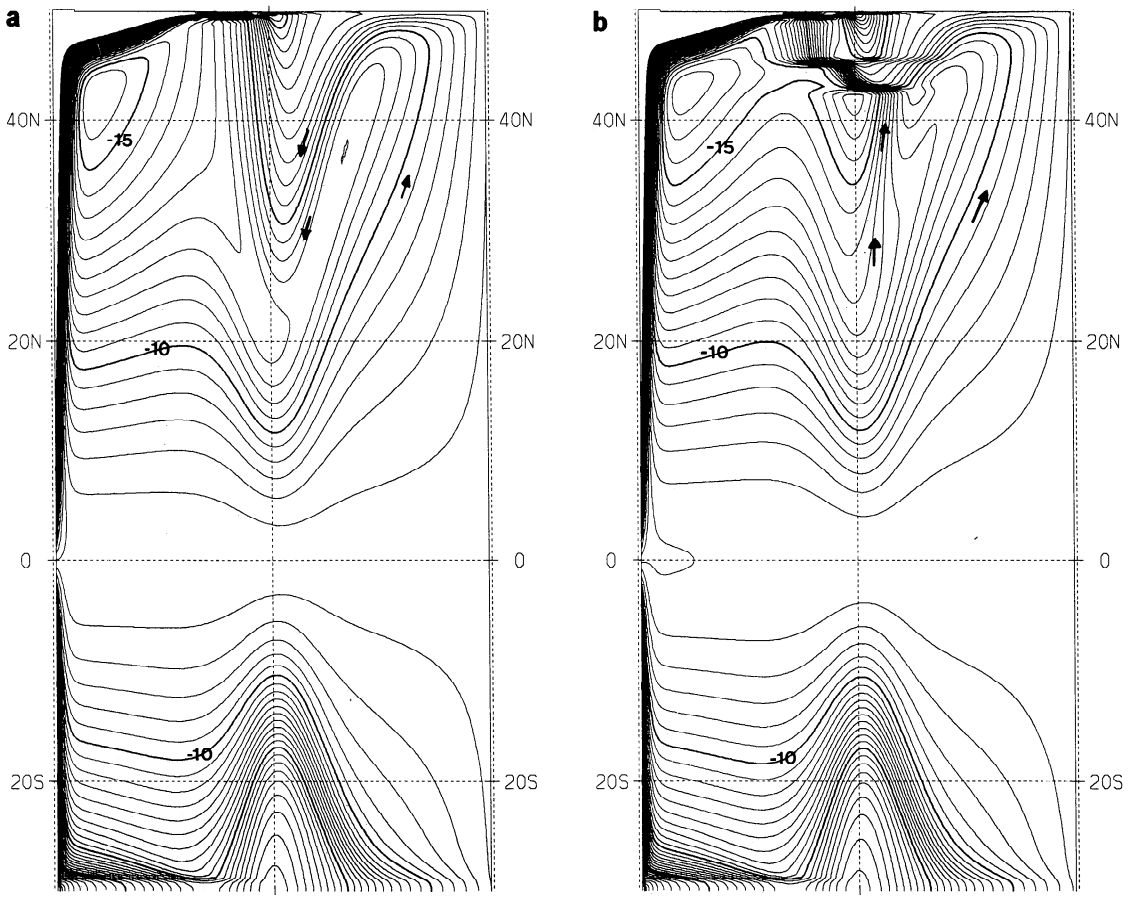

Figure 5. The box-shaped ocean with a Gaussian ridge. Contours of the steady state interface displacement (day 10800) for (a) the meridional ridge and for (b) the ridge with a gap. The contour interval is 0.5 m, the contours are labeled in units of meters.

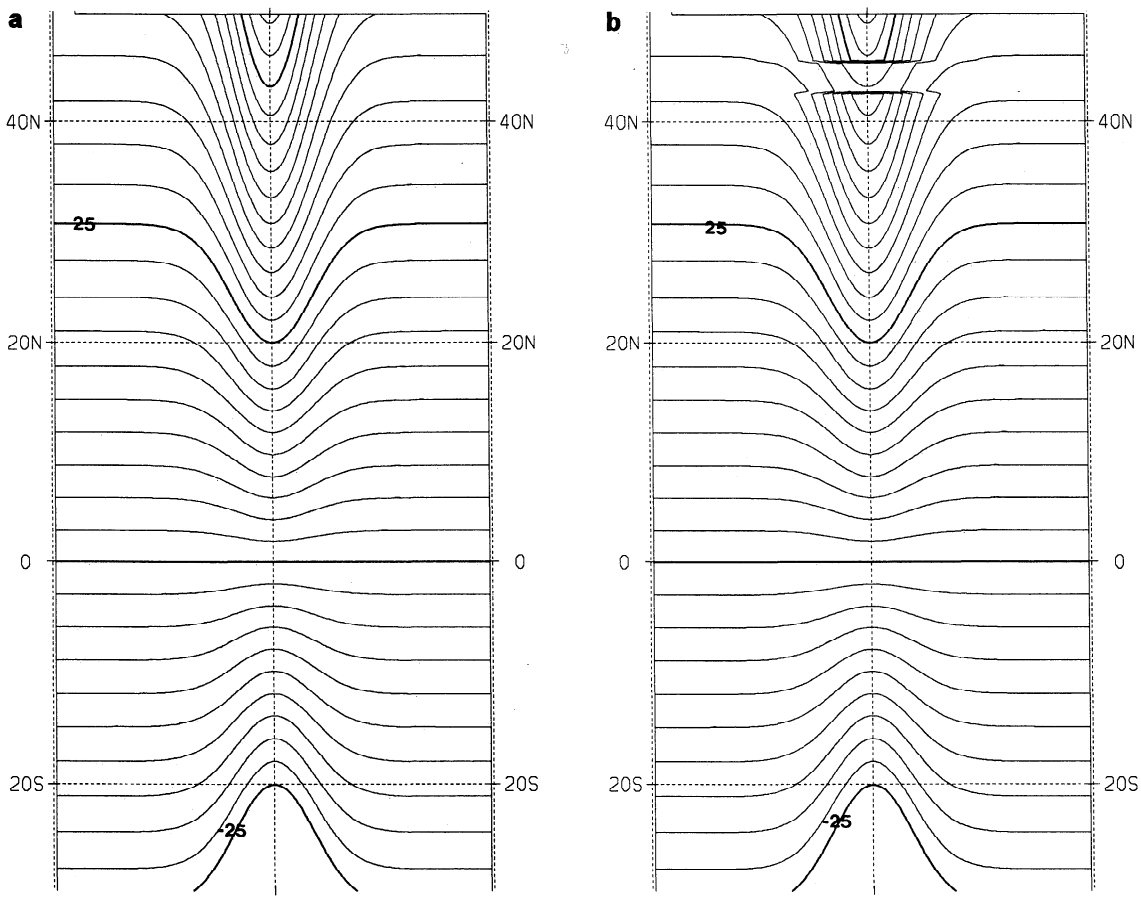

Figure 6. Geostrophic contours of the box-shaped ocean (a) with a meridional ridge and (b) with the same ridge including a gap at high latitudes. The contour labels give the isoline values in units of $10^{-9}(\mathrm{sm})^{-1}$ at an interval of $2.5 \times 10^{-9}(\mathrm{sm})^{-1}$.

boundary current up to ≈30°N and continues as an intensified flow along the eastern boundary north of 32°N. According to *McCartney* [1992] this Lower Deep Water (LDW) is the source of the DNBC which, enhanced by the Greenland-Scotland overflows, is the origin of the DWBC. Figure 4b shows the steady state flow in the North Atlantic presented as current vectors from our model results. It is obvious that the bulk of the water circulating in the eastern basin enters across the Mid-Atlantic Ridge between 10° and 14°N. In fact, part of the ridge current crosses the basin north of 30°N and intensifies the eastern slope current. This current turns west along the northern boundary and joins the inflow from the Denmark Strait to flow south as the DWBC in the western basin (Figure 7). The vorticity balance of the midlatitude zonal flows connecting the ridge current and the eastern slope current is dominated by local upwelling, friction, and topography.

The Antarctic Bottom Water (AABW) which crosses the equator into the western basin takes a similiar turn toward the eastern boundary. *Speer and McCartney* [1992] find that a grounding of the interface, through which the AABW upwells into the lower North Atlantic Deep Water, occurs. In their flat bottom model the grounding line guides the flow toward the east. *McCartney* [1992] applies this idea to the situation of the LDW in the Northeast Atlantic also. The grounding interface mechanism is absent in our model. Here the topographic control guides the flow to the east.

Dickson et al. [1985] tried to infer the mean deep-circulation patterns in the Madeira, Iberia, and Porcupine Abyssal Plains from long-term current measurements below 2000 m depth. Over the Porcupine Abyssal Plain they found a cyclonic gyre with an intense current following the continental slope. Similiar features can be seen in the model result shown in Figure 7. Their data give no coherent flow pattern for the other two basins. However, the northeastward flow along the Azores-Portugal Ridge and over the Madeira Abyssal Plain and the westward flow over the Iberia Abyssal Plain fit to the direction of flow in the current-meter data, indicating topographic guidance of the flow. The current-meter data could not provide a clear picture of the flow field along the eastern flank of the Mid-Atlantic Ridge. However, because of the rough topography of the ridge it is generally difficult to infer the large-scale flow pattern from current-meter data (E. Mittelstaedt, personal communication, 1992).

Figure 8 shows the steady state flow field for the Mid-Atlantic Bight. The current vectors follow the structure of the recirculation cell fed by a broad bifurcation of the DWBC between 25° and 35°N. Southeast of the

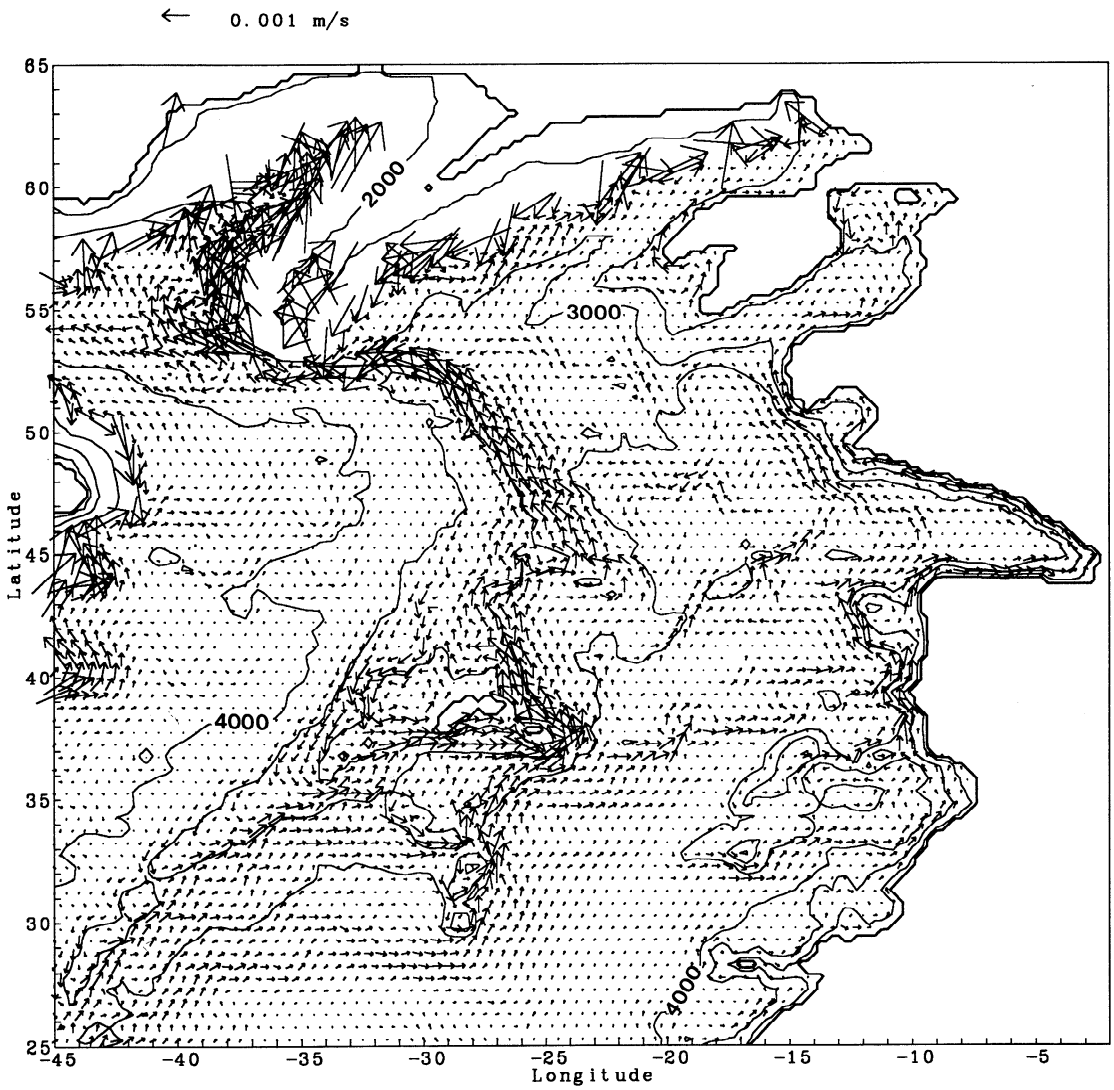

Figure 7. Current velocities in the Northeast Atlantic on day 9600 (steady state). The thin lines are the depth contours at an interval of 1000 m. Velocities in excess of 3×10^{-3}m/s have been omitted.

Bermudas and the New England Seamounts the recirculation is most intense. A small fraction recirculates into the DWBC just west of the seamounts, the rest closes the gyre south of Newfoundland. To obtain the mean current field, *Hogg* [1983] and *Hogg et al.* [1986] compiled a number of deep current-meter data from this area. Away from the DWBC the compiled data record a patchy structure with many small-scale features. More conspicious is an elongated recirculation cell centered north of the Gulf Stream axis at 40°N, 57°W. Numerous studies found strong interactions between the Gulf Stream and the adjacent deep flow [e.g., *Hogg and Stommel*, 1985; *Thompson and Schmitz*, 1989; *Bower and Hogg*, 1992]. Thus we expected only poor agreement between our $1\frac{1}{2}$-layer model flow and the measurements. In fact, the overall comparison with the data is less favorable than for the Northeast Atlantic, though a weak cyclone centered at 40°N, 57°W can be seen in Figure 8.

Generally, the model velocities are an order of magnitude smaller than the current meter data. One possible explanation may be that the abyssal currents are more bottom trapped than our $1\frac{1}{2}$-layer model can allow. A second reason might be the strength of the interior recirculation, which is a result of the intensity of the upwelling. In reality, the interaction between the bottom relief and interior dynamics might enhance vertical eddy diffusivity along strong bottom slopes [*McDougall*, 1989]. Such an enhancement of the k_d values in fact leads to intensified flows in these areas [*Karcher et al.*, 1990] .

Breakdown

With this experiment we examine the response of the circulation to a reduction of inflow into the deep water. It is motivated by several studies which gave evidence of changes in the water masses south of the

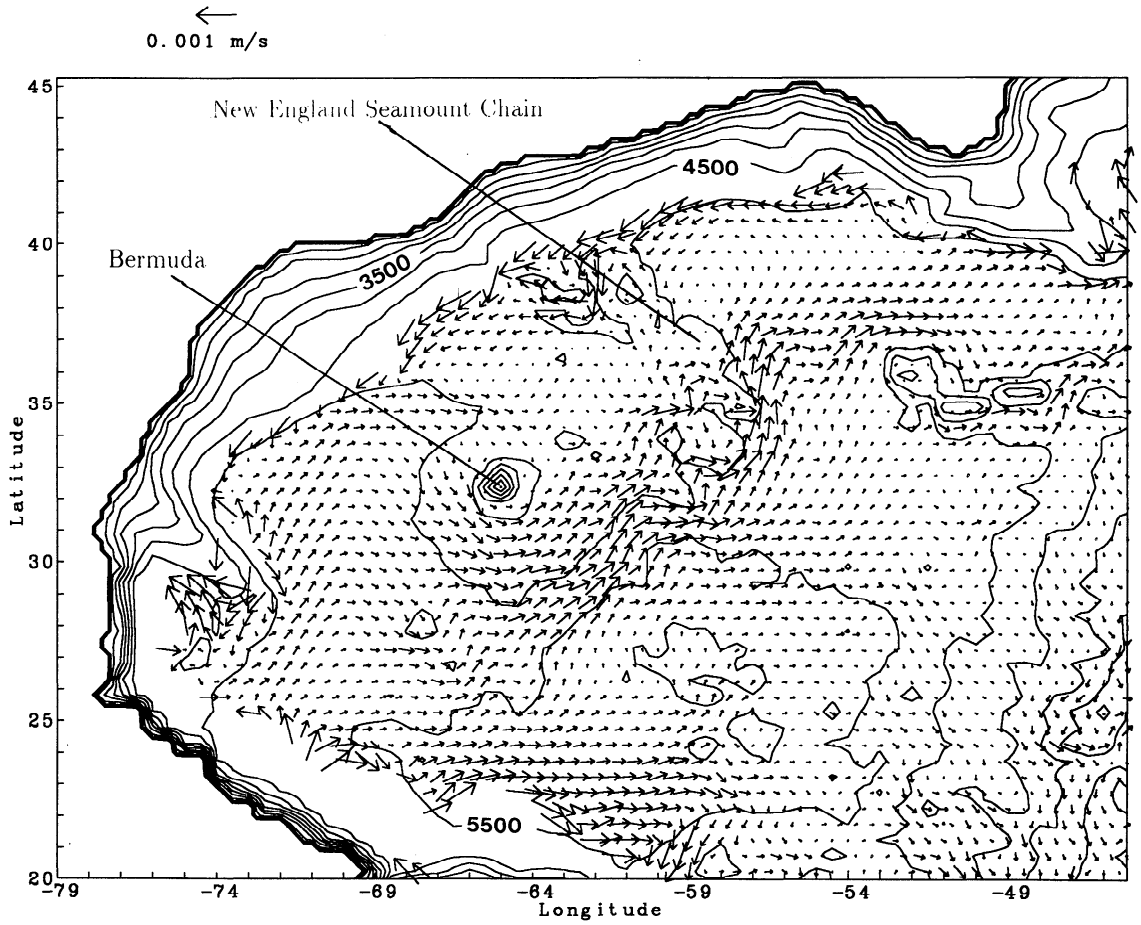

Figure 8. Current velocities in the Mid-Atlantic Bight on day 9600 (steady-state). Every second current vector has been plotted. The thin lines are depth contours with an interval of 500 m. Velocities in excess of 1×10^{-3}m/s have been omitted.

Greenland-Scotland ridges induced by variations in the properties of overflow water [*Swift*, 1984; *Lazier*, 1988]. It is well known that the production rate of deep water in the polar oceans is not constant [e.g., *Smethie et al.*, 1986; *Meincke et al.*, 1992]. We definitely know that changes in the production of Labrador Sea Water affect the DWBC [*Talley and McCartney*, 1982]. *Dickson et al.* [1990] and *Saunders* [1990], on the other hand, found no seasonal or interannual fluctuations of inflows through the Denmark Strait and through the Faroe Bank Channel. It remains an open question, as to how to explain the incompatibility between a fluctuating production of dense deep water and a constant outflow. In the 1970s an extraordinary event occurred in the regime of the subpolar North Atlantic. The Great Salinity Anomaly prohibited deep convection in several regions [*Dickson et al.*, 1988]. Such an event should also have a strong impact on the inflow of deep water into the North Atlantic.

Circulation after the Breakdown

We start from the steady state (ST = day 9600), reduce the inflow volume through the Denmark Strait by 90% of the steady state volume in a 300-day period, and keep this reduced value thereafter. The inflow volume between Iceland and Scotland remains constant. Figure 9a shows the circulation 400 days after the onset of reduction (day ST+400). The arrows indicate the flow direction. The circulation pattern has not yet changed in the western and northwestern part of the ocean away from the DWBC. The ridge current is still poleward north of 20°N. The whole circulation in the eastern basin, however, has changed drastically. The perturbation, carried by long Rossby waves, crosses the ocean as a meridionally elongated anticyclonic gyre that reverses the poleward interior flow to an equatorward flow in its wake. On day ST+600 (Figure 9b) the perturbation has crossed the Mid-Atlantic Ridge and a reversal of flow direction can also be observed in the southeastern area of the western basin. Figure 9c shows the circulation on day ST+800. Along the equator and behind a basinwide cyclonic gyre which moves across the basin, the flow pattern of the steady state is established again. With the exception of the northern Mid-Atlantic Bight the perturbation reverses the flow direction in the entire interior western basin. The strong ridge current and the flow in the southeastern part of the CGFZ have disappeared. Later in the evolution the circulation pattern of the steady state returns when the perturbation has

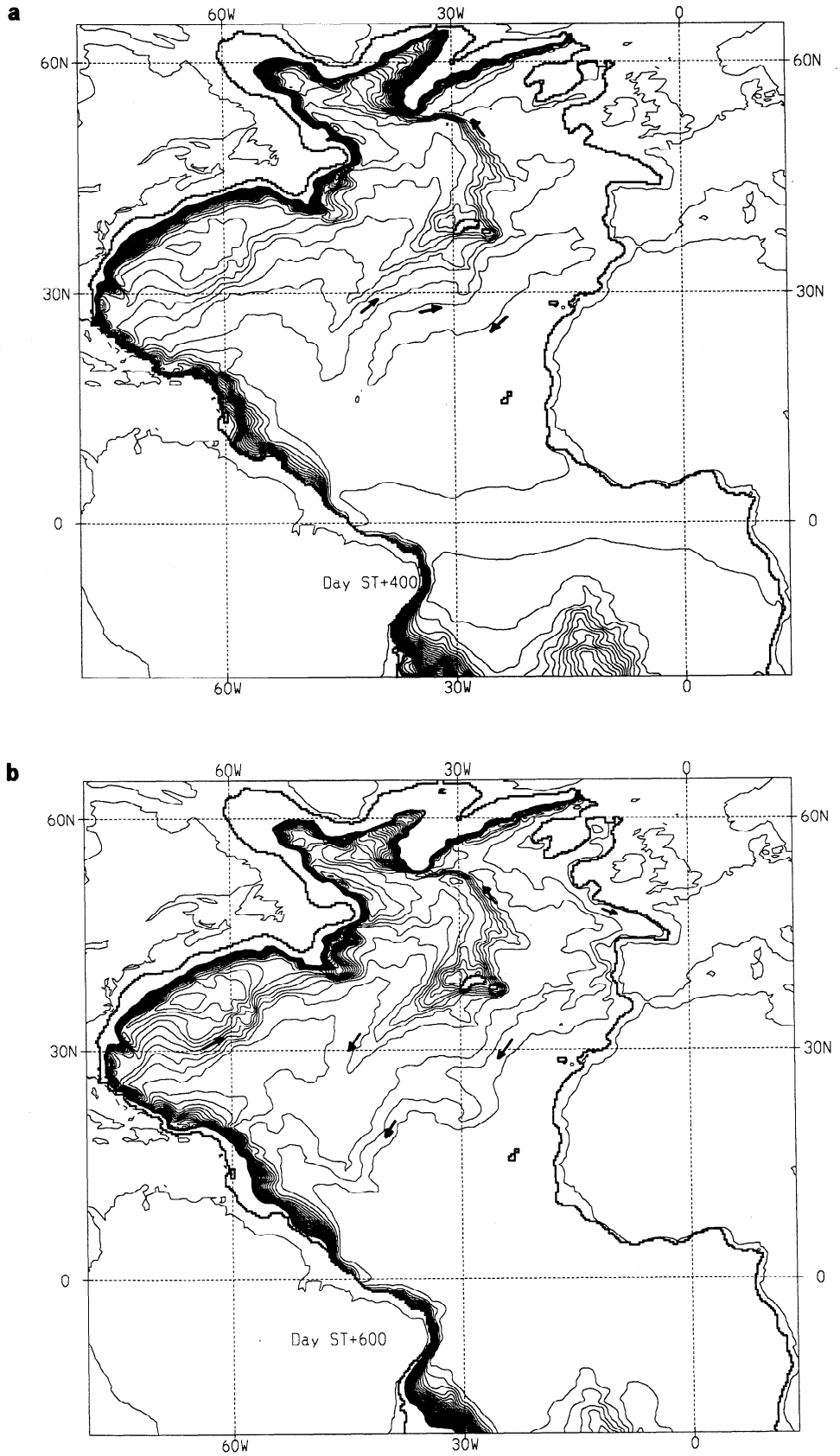

Figure 9. The breakdown. Lines of constant interface displacement. The vectors indicate the direction of flow. (a) Day ST+400, 400 days after the onset of the inflow reduction. Contours in meters at an interval of 0.5 m. Lines in excess of 10 m have been omitted. (b): Day ST+600 and (c) day ST+800, 600 and 800 days after the onset of the inflow reduction, respectively. Contours in meters at an interval of 0.2 m. Lines in excess of -3 m have been omitted.

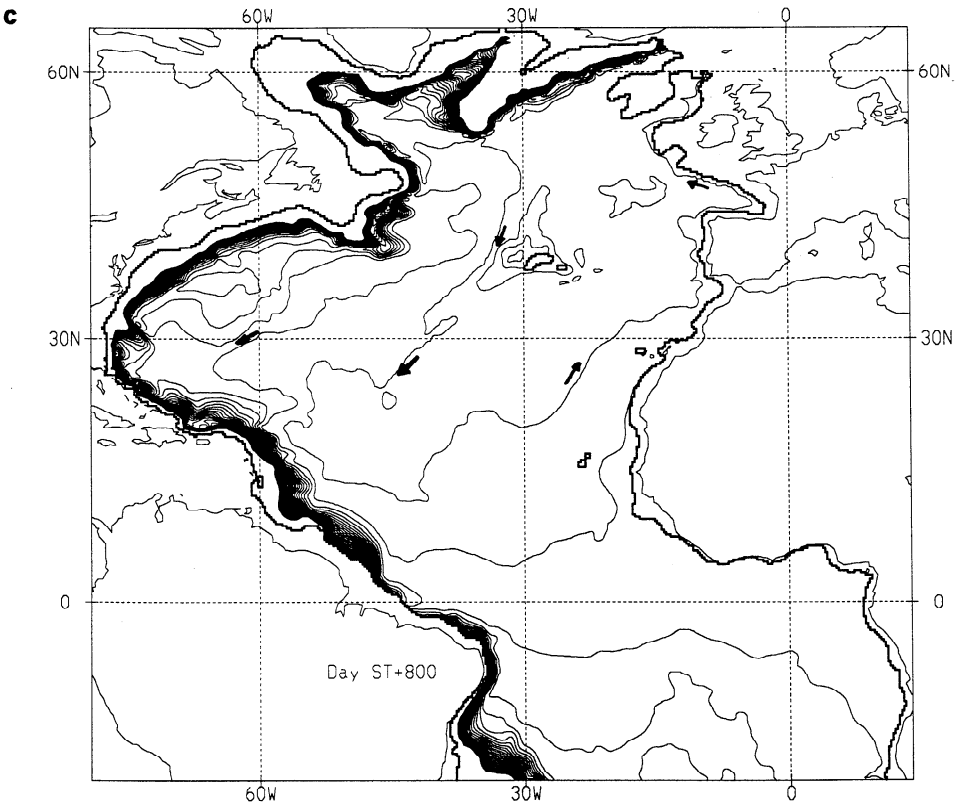

Figure 9. (continued)

passed, although now with a reduced intensity because of the smaller inflow volume. The reduction of the inflow leads to an imbalance in the basinwide mass balance. The imbalance causes the interface to sink until the cross-interfacial flux again balances the difference between inflow and outflow. The squeezing of the water column induces an equatorward interior flow until the upward velocity through the interface outbalances the sinking of the interface and the net vertical velocity is upward again.

Distribution of Response Time Regimes

During the spin-up the inflow had developed to its full strength in 50 days starting from an ocean at rest. For the breakdown the total inflow had been reduced by ≈60% (DSOW by 90%) in 300 days, starting from the steady state circulation. Thus the perturbations and their timescales are different for the two experiments. Nonetheless, the path and the velocity of perturbations are very similiar in both cases and so are the arrival times of the perturbations at certain locations. These response time regimes are shown in Figure 10 for the breakdown experiment. Note that an interface displacement of 5×10^{-2} m from the steady state, and not the peak distortion, has been chosen to indicate the arrival of the perturbation.

In the first stage the perturbation travels by fast-moving coastal Kelvin waves and arrives first at the western and eastern boundaries and at the equator. In the interior the relation between the group velocity of the long baroclinic Rossby waves and the distance along the travel path determines the time of arrival for a signal starting at the boundary [*Straub and Rhines*, 1990]. The group velocity, $v_g = \beta R_{\text{def}}^2$, is proportional to the density stratification, which allows an estimate of the travel times for different stratifications. In the interior a zonal propagation of the perturbation signal across the ridge is possible only at low latitudes and through the CGFZ. All other geostrophic contours starting at the eastern boundary turn toward the equator, cross the ridge, and then turn to the north (Figure 1b). This pattern of the geostrophic contours puts the northwestern part of the Atlantic in the shadow of the Mid-Atlantic Ridge, and distances along contours reaching the Northwest Atlantic are extremely long. It takes more than a year before the perturbation reaches the area northwest of Madeira.

Summary and Discussion

The time dependent behavior of the dynamics of the deep North Atlantic ocean is investigated. For this purpose we have used a $1\frac{1}{2}$-layer reduced gravity model with a spatial resolution of 0.25°. The model is driven by an inflow at the northern boundary and a flux through the interior interface.

In contrast to similiar previous studies a realistic topography and an open southern boundary have been

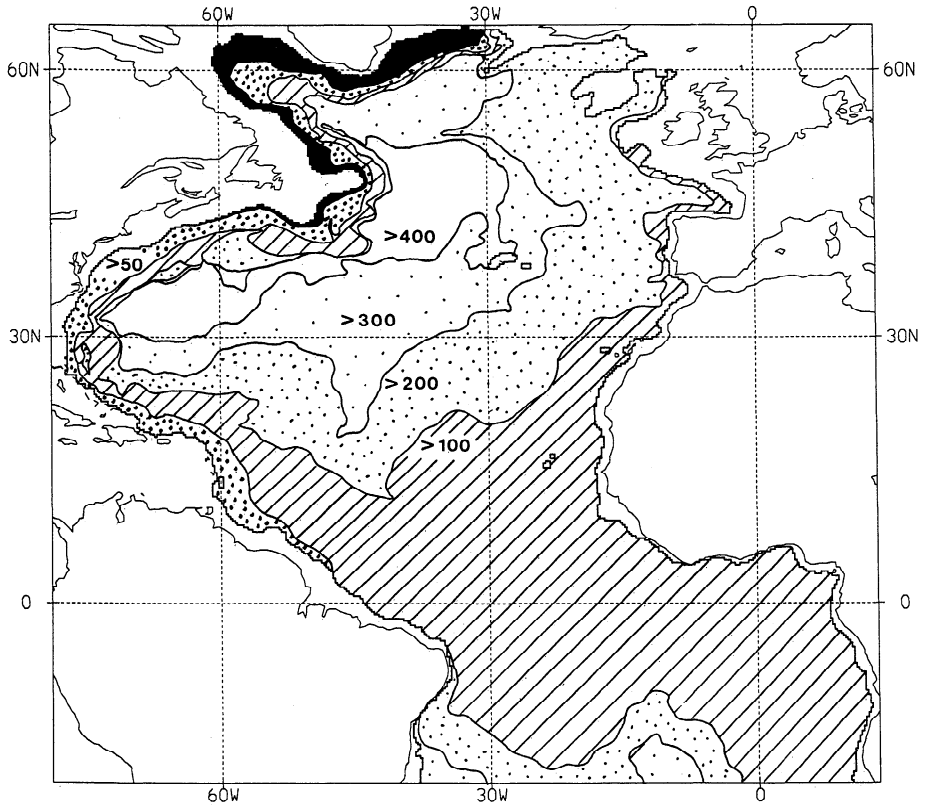

Figure 10. The response time regimes for the breakdown experiment. The contours denote the line to which the perturbation has traveled on days 50, 100, 200, 300, and 400 after the onset of the inflow reduction, the black area has been covered in less than 50 days.

taken into account. Furthermore, a damping timescale for the long baroclinic Rossby waves has been introduced which allows a full development of the interior circulation. The relatively high horizontal resolution of our numerical model has been chosen in particular to resolve the internal Rossby radius.

The resulting stationary flow pattern reveals a complex structure. An important difference from the flat bottom Stommel-Arons circulation is the recirculating northward flow along the eastern boundary fed by intense zonal jets in the interior. Their pathways are determined jointly by spatial variations of the interface flux and by topographic effects. We have also found a strong northward current along the eastern slope of the Mid-Atlantic Ridge that is fed by the DWBC and recirculates into the western basin across the CGFZ. In an earlier study, *Welander* [1969] postulated a southward ridge current. By means of an idealized box-shaped model we have shown that the direction of the ridge current depends on the existence of a gap at high latitudes, a CGFZ analogue.

Our model completely neglects an upper-layer flow and momentum coupling across the interface. Consequently the agreement with observations of deep currents is particularly poor in areas where in reality a close interaction (e.g., between the upper-layer flow and the deep flow) has to be anticipated, such as the Gulf Stream region.

For the eastern part of the deep North Atlantic, however, we have found good agreement of the model flow pattern with observations. This indicates that topography plays a major role and that the time average deep currents in the eastern North Atlantic may be less affected by the surface circulation. Model velocities in the interior ocean are small compared to measurements. Possible reasons have been discussed.

We have performed spin-up and breakdown experiments, gradually increasing and decreasing the forcing inflow volume to its final constant value. The spin-up experiment starts from an ocean at rest. The spin-down experiment is initialized with the resulting quasi steady state of the spin-up. These experiments provide information on the spatial distribution of typical response time regimes. In both cases, information transfer takes similiar routes. Seperate regimes could be distinguished and classified according to their response timescales. It turns out that the interior northwest close to the inflow source is characterized by the latest arrival time of a perturbation.

We feel that our model is a valuable tool for further studies of deep sea dynamics. Several aspects of deep flow dynamics controlled by realistic topography will be adressed in forthcoming investigations. The effect of fluctuating inflow from different deep water sources in the North Atlantic will be a subject of a future study with this model. The interaction between time depen-

dent flows above and below the thermocline will be given further attention. Also the intruding AABW interacts with the NADW circulation above. In this context we plan to generalize our model for the simulation of three moving layers.

Appendix

We want to make some remarks on the choice of the value of k_d, which has been chosen here to be $k_d = 2 \times 10^{-3}\mathrm{m}^2/\mathrm{s}$. Compared to $k_d \approx 1 \times 10^{-4}\mathrm{m}^2/\mathrm{s}$ (commonly used in general circulation models) or estimates from in situ experiments and inverse calculations of $k_d \leq 1 \times 10^{-5}\mathrm{m}^2/\mathrm{s}$ [*Gregg*, 1987; *Olbers et al.*, 1985], our value is relatively large.

According to (11) the value of k_d determines the value of λ which governs the damping of the long Rossby waves. Equation (11) gives a damping timescale $\tau_\lambda = \lambda^{-1} = 3000$ days for the chosen set of model parameters. *Kawase* [1987] introduced the parameter $\delta = \frac{\beta R_{\mathrm{def}}^2}{\lambda L}$, which is the ratio of the damping timescale λ^{-1} to the long Rossby wave travel time across a model ocean of length scale L. The value of δ determines whether the Rossby waves are able to cross the ocean completely ($\delta \geq 1$) or are damped out before ($\delta < 1$). In the latter case the establishment of the interior circulation is not complete.

A k_d much smaller than $2 \times 10^{-3}\mathrm{m}^2/\mathrm{s}$, however, would imply damping timescales of the order of 100 to 1000 years. This would require an enormous additional computation time to reach the steady state. On the other hand, $k_d = 2 \times 10^{-3}\mathrm{m}^2/\mathrm{s}$ is sufficently small to ensure $\delta \geq 1$ at all latitudes. In the case of a realistic bottom topography the calculation of δ is not straightforward, since the Rossby waves follow curved paths. Time series of the current velocities in the western basin show, however, that in the present experiment Rossby waves are able to cross the basin several times before they are damped out. This is also illuminated by the distribution of response time regimes as shown in Figure 10. In addition, spin-up experiments with $k_d < 2 \times 10^{-3}\mathrm{m}^2/\mathrm{s}$ showed no significant differences of the flow pattern compared to the spin-up of the present experiment with $k_d = 2 \times 10^{-3}\mathrm{m}^2/\mathrm{s}$.

The large k_d, however, produces large fluxes across the interface because the cross-interfacial velocity is proportional to k_d (7). To overcome this difficulty, the two terms contributing to the linearized interfacial velocity (10) are treated differently. The term e_0, which does not depend on the model flow, is prescribed as a uniform background velocity, instead of beeing calculated according to (12). The damping term $\lambda\eta$, which depends on the interface displacement η, is calculated according to (10) and (11).

By these means and the use of $k_d = 2 \times 10^{-3}\mathrm{m}^2/\mathrm{s}$, a sensible overall volume flux through the interface, a complete spin-up of the interior circulation, and an approach to a steady state can be achieved.

Acknowledgments. The authors would like to thank Mitsuhiro Kawase and an anonymous reviewer for their helpful comments and fruitful suggestions. We are also grateful to Hans Friedrich for revising the manuscript.

The work was funded by the Deutsche Forschungsgemeinschaft DFG as a part of the program SFB 318 'Klimarelevante Prozesse im System Ozean - Atmosphäre - Kryosphäre'.

References

Bower, A.S., and N.G. Hogg, Evidence for barotropic wave radiation from the Gulf Stream, *J.Phys.Oceanogr., 22*, 42-61, 1992

Cessi, P., and J. Pedlosky, On the role of topography in the ocean circulation, *J.Mar.Res., 44*, 445-471, 1986

Condie, S.A., and M. Kawase, Models of abyssal flow in basins separated by a mid-ocean ridge, *J.Mar.Res., 50*, 421-440, 1992

Dickson, R.R., W.J. Gould, T.J. Müller, C. Maillard, Estimates of the mean circulation in the deep (> 2000 m) layer of the eastern North Atlantic, *Prog. Oceanogr., 14*, 103-127, 1985

Dickson, R.R., J. Meincke, S.-A. Malmberg, and A.J. Lee, The 'Great Salinity Anomaly' in the northern North Atlantic, *Prog. Oceanogr., 20*, 103-151, 1988

Dickson, R.R., E.M. Gmitrowicz, and A.J. Watson, Deep water renewal in the northern North Atlantic, *Nature, 344*, 848-850, 1990

Gargett, A.E., Vertical eddy diffusivity in the ocean interior, *J.Mar.Res., 42*, 359-393, 1984

Gregg, M.C., Diapycnal mixing in the thermocline: A review, *J.Geophys.Res., 92*, 5249-5286, 1987

Hautala, S.L., and S.T. Riser, A simple model of abyssal circulation, including effects of wind, buoyancy, and topography, *J.Phys.Oceanogr., 19*, 596-611, 1989

Hogg, N.G., A note on the deep circulation of the western North Atlantic: Its nature and causes, *Deep Sea Res., 30*, 945-961, 1983

Hogg, N.G., and H. Stommel, On the relationship between the deep circulation and the Gulf Stream, *Deep Sea Res., 32*, 1181-1193, 1985

Hogg, N.G., R.S. Pickart, R.M. Hendry, and W.J. Smethie Jr., The northern recirculation gyre of the Gulf Stream, *Deep Sea Res., 33*, 1139-1165, 1986

Joyce, T.M., and K.G. Speer, Modeling the large-scale influence of geothermal sources on abyssal flow, *J.Geophys.Res., 92*, 2843-2850, 1987

Karcher, M., A. Lippert, and P. Müller, The influence of spacially varying eddy-diffusivity on the deep circulation (abstract), *Ann.Geophys., 8*, 129, 1990

Kawase, M., Establishment of deep ocean circulation driven by deep-water production, *J.Phys.Oceanogr., 17*, 2294-2317, 1987

Kawase, M., Effects of a concave bottom geometry on the upwelling-driven circulation in an abyssal ocean basin, *J.Phys.Oceanogr., 23*, 400-405, 1993

Kawase, M., and D. Straub, Spinup of source-driven circulation in an abyssal basin in the presence of bottom topography, *J.Phys.Oceanogr., 21*, 1501-1514, 1991

Lazier, J.R., Temperature and salinity changes in the deep Labrador Sea, 1962-1986, *Deep Sea Res., 35*, 1247-1253, 1988

Levitus, S., Interpentadal variability of temperature and salinity in the deep North Atlantic, 1970-1974 versus 1955-1959, *J.Geophys.Res., 94*, 16,125 - 16,131, 1989

McCartney, M.S., Recirculating components to the deep boundary current of the northern North Atlantic, *Prog. Oceanogr., 29*, 283-383, 1992

McCartney, M.S., S.L. Bennett, and M.E. Woodgate-Jones, Eastward flow through the Mid-Atlantic Ridge at 11°N and its influence on the abyss of the eastern basin, *J.Phys.Oceanogr., 21*, 1089-1121, 1991

McDougall, T.J., Dianeutral advection, in,*'Aha Huliko'a, Proceedings of the Hawaiian Winter Workshop on Parameterization of small-scale processes*, pp. 289-315, University of Hawaii at Manoa, 1989

Meincke, J., S. Jónsson, and J.H. Swift, Variability of convective conditions in the Greenland Sea, *ICES Mar.Sci.Symp., 195*, 32-39, 1992

Olbers, D.J., M. Wenzel, and J. Willebrand, The inference of North Atlantic circulation patterns from climatological hydrographic data, *Rev.Geophys., 23*, 313-356, 1985

Pedlosky, J., *Geophysical Fluid Dynamics*, 2nd ed., Springer-Verlag, New York, 1987

Roemmich, D., and C. Wunsch, Apparent changes in the climatic state of the deep North Atlantic Ocean, *Nature, 307*, 447-450, 1984

Sadourny, R., Compressible model flows on the sphere, *J.Atmos.Sci., 32*, 2103-2110, 1975

Saunders, P.M., Cold outflow from the Faroe Bank Channel, *J.Phys.Oceanogr.*, 20, 29-43, 1990

Simons, T.J., Circulation models of lakes and inland seas, *Can. Bull. Fish. Aquat. Sci., 203*, 22-31, 1980

Smethie, W.M., Jr., H.G. Ostlund, and H.H. Loosli, Ventilation of the deep Greenland and Norwegian seas: Evidence from krypton-85, tritium, carbon-14, and argon-39, *Deep Sea Res., 33*, 675-703, 1986

Speer, K.G., and M.S. McCartney, Bottom water circulation in the western North Atlantic, *J.Phys.Oceanogr., 22*, 83-92, 1992

Stommel, H., and A.B. Arons, On the abyssal circulation of the world ocean - I. Stationary planetary flow patterns on a sphere, *Deep Sea Res., 6*, 140-154, 1960

Straub, D.N., and P.B. Rhines, Effects of large-scale topography on abyssal circulation, *J.Mar.Res., 48*, 223-253, 1990

Swallow, J.C., and L.V. Worthington, An observation of a deep counter-current in the western North Atlantic, *Deep Sea Res., 8*, 1-19, 1961

Swift, J.H., A recent θ-S shift in the deep water of the northern North Atlantic, in *Climate Processes and Climate Sensitivity*, edited by J.E. Hansen and T. Takahashi, AGU, Washington D.C., *Geophys. Monogr., Ser. 5, Vol. 29*, pp. 39-47, 1984

Talley, L.D., and M.S. McCartney, Distribution and circulation of Labrador Sea Water, *J.Phys.Oceanogr., 12*, 1189-1205, 1982

Thompson, J.D., and W.J. Schmitz, A limited-area model of the Gulf Stream: Design, initial experiments, and model-data intercomparison, *J.Phys.Oceanogr., 19*, 791-813, 1989

Tziperman, E., On the role of interior mixing and air-sea fluxes in determining the stratification and circulation of the oceans, *J.Phys.Oceanogr., 16*, 680-693, 1986

Welander, P., Effects of planetary topography on the deep-sea circulation *Deep Sea Res., 16*, 369-391, 1969

M. Karcher and A. Lippert, Institut für Meereskunde, Universität Hamburg, Troplowitzstrasse 7, 22529 Hamburg, Germany.

(Received December 10, 1992; revised May 27, 1993; accepted September 15, 1993.)